CSIRO PUBLISHING

Publications of the Astronomical Society of Australia, 2012, **29**, 121–131
http://dx.doi.org/10.1071/AS11078

Transformations from *WISE* to 2MASS, SDSS and *BVI* Photometric Systems: II. Transformation Equations for Red-Clump Stars

S. Bilir[A,E], *S. Karaali*[A], *N. D. Dağtekin*[A], *Ö. Önal*[A], *S. Ak*[A], *T. Ak*[A], *and A. Cabrera-Lavers*[B,C,D]

[A]Istanbul University, Faculty of Sciences, Department of Astronomy and Space Sciences, 34119 University, Istanbul, Turkey
[B]Instituto de Astrofísica de Canarias, E-38205 La Laguna, Tenerife, Spain
[C]GTC Project Office, E-38205 La Laguna, Tenerife, Spain
[D]Departamento de Astrofísica, Universidad de La Laguna, E-38205 La Laguna, Tenerife, Spain
[E]Corresponding author. Email: sbilir@istanbul.edu.tr

Abstract: We present colour transformations for the conversion of *Wide-Field Survey Explorer* $W1$, $W2$, and $W3$ magnitudes to the Johnson–Cousins BVI_c, Sloan Digital Sky Survey *gri*, and Two Micron All Sky Survey JHK_s photometric systems, for red clump (RC) stars. RC stars were selected from the Third Radial Velocity Experiment Data Release. The apparent magnitudes were collected by matching the coordinates of this sample with different photometric catalogues. The final sample (355 RC stars) was used to obtain metallicity-dependent and free-of-metallicity transformations. These transformations combined with known absolute magnitudes at shorter wavelengths can be used in space density determinations for the Galactic (thin and thick) discs at distances larger than the ones evaluated with JHK_s photometry alone, hence providing a powerful tool in the analysis of Galactic structure.

Keywords: techniques: photometric — catalogues — surveys

Received 2011 December 26, accepted 2012 February 2, published online 2012 March 6

1 Introduction

Red clump (RC) stars are core helium-burning stars, in an identical evolutionary phase to that of stars on the horizontal branch in globular clusters. However, in intermediate- and higher-metallicity systems only the red end of the distribution is seen, forming a clump of stars in the colour–magnitude diagram. In recent years much work has been devoted to studying the suitability of RC stars as a distance indicator. Their absolute magnitude in the optical ranges from $M_V = +0.70$ mag for those of spectral type G8 III to $M_V = +1.0$ mag for the K2 III ones (Keenan & Barnbaumet 1999). The absolute magnitude of these stars in the K_s band is $M_{K_s} - 1.54 \pm 0.04$ mag with negligible dependence in metallicity (Groenewegen 2008). The optical and infrared colour ranges for these stars are $0.8 \leq (B-V)_0 \leq 1.3$ and $0.29 \leq (J-H)_0 \leq 0.65$, respectively, and they have a limited surface gravity, i.e. $2.1 \leq \log g \leq 2.7$ cm s^{-2} (Puzeras et al. 2010).

It should be added that RC stars are different in structure than the ones in late transitional phases of evolution off the main sequence or immediately before a supernova, which have circumstellar material, i.e. red supergiants, yellow hypergiants, luminous blue variables, B[e] supergiants and equatorial rings, interacting binaries and Wolf–Rayet stars.

In a former paper (Bilir et al. 2011a, hereafter Paper I) we presented the transformation equations from *Wide-Field Survey Explorer WISE* to Two-Micron All-Sky Survey (2MASS), Sloan Digital Sky Survey (SDSS) and Johnson–Cousins photometric systems for dwarf stars. Here, our aim is to obtain similar transformations between the same photometric systems but for RC stars. The galactic model parameters can be obtained more precisely using *WISE* absolute magnitudes calculated from these transformations. In the next paragraphs, we give a short definition for the mentioned photometric systems and the Wide-Field Survey Explorer (*WISE*) survey, which provides the data used in our study. However, we refer the reader to Paper I for a more complete information.

The SDSS obtains images almost simultaneously in five broad bands (u, g, r, i, and z) centered at 3560, 4680, 6180, 7500 and 8870 Å, respectively, (York et al. 2000). The magnitudes derived from fitting a point spread function (PSF) are currently accurate to about 1% in g, r, i, z and 2% in u for point sources (Padmanabhan et al. 2008). The data have been made public in a series of yearly data release where the eighth data release (DR8, Aihara et al. 2011) covers 14 555 deg^2 of imaging area. The limiting magnitudes are $(u, g, r, i, z) = (22, 22.2, 22.2, 21.3, 20.5)$.

The 2MASS (Skrutskie et al. 2006) provides the most complete data base of near infrared (NIR) Galactic point sources available to date. Observations cover 99.998% (Skrutskie et al. 2006) of the sky with simultaneous detections in J (1.25 μm), H (1.65 μm), and K_s (2.17 μm) bands up to the limiting magnitudes of 15.8, 15.1, and 14.3, respectively. Bright source extractions have 1σ photometric uncertainty of <0.03 mag and astrometric accuracy on the order of 100 mas.

The *WISE* (Wright et al. 2010), an up-to-date infrared (IR) satellite, began surveying the sky on 2010 January 14 and completed its first full coverage of the sky on 2010 July 17 with much higher sensitivity than comparable previous IR survey missions. *WISE* has four IR filters $W1$, $W2$, $W3$, and $W4$ centered at 3.4, 4.6, 12, and 22 μm, and with the angular resolutions 6.1, 6.4, 6.5, and 12 arcsec, respectively and has a 40-cm telescope feeding array with a total of four million pixels. *WISE* has achieved 5σ point-source sensitivities better than 0.08, 0.11, 1 and 6 mJy at 3.4, 4.6, 12, and 22 μm, respectively. These sensitivities correspond to the Vega magnitudes 16.5, 15.5, 11.2, and 7.9. Thus *WISE* will go a magnitude deeper than the 2MASS K_s data in $W1$ for sources with spectra close to that of an A0 star, and even deeper for moderately red sources like K stars or galaxies with old stellar populations.

The RAVE (Steinmetz et al. 2006) measures radial velocities and stellar atmospheric parameters from spectra using the 6dF multi-object spectrometer on the Anglo–Australian Astronomical Observatory's 1.2-m UK Schmidt Telescope. The survey looks in the Ca-triplet region (8410–8795 Å), has a resolution of ~7500, and is magnitude limited. The targets chosen are Southern Hemisphere stars taken from the *Tycho-2*, SuperCOSMOS and the Deep Near Infrared Survey of the Southern Sky (DENIS, Fouque et al. 2000) surveys with I-band magnitudes between 9 and 13. The average internal errors in radial velocity are $\sim 2\,\mathrm{km\,s^{-1}}$, and the approximate radial velocity offset between the RAVE and the literature is smaller than $\sim 1\,\mathrm{km\,s^{-1}}$. The catalogue also includes 2MASS photometry and proper motions from Starnet 2.0, *Tycho-2*, SuperCOSMOS, and UCAC2 (for more information about RAVE, see Zwitter et al. 2008).

The passband profiles for the Johnson–Cousins, SDSS, 2MASS, and *WISE* photometric systems are shown in Figure 1. With respect to the same figure in Paper I, we omitted here the passband for R which is not used in our transformations but we added the DENIS passband I_d with which we evaluated the Cousins optical magnitudes (I). $W3$ and $W4$ could not be used in Paper I in the transformations for dwarfs due to the faintness of dwarfs in both bands. In this study of RC stars, the $W3$ magnitudes could be used but the $W4$ magnitudes were too faint. Hence, as in the inverse transformations for dwarfs, the $J - H$ colour of the 2MASS photometric system is used as a second colour combined linearly with $W1 - W2$. Figure 2 plots the fields available with the *WISE* and RAVE surveys.

In Section 2 we present the sources of our sample and the criteria applied to the chosen stars. The transformation equations are given in Section 3 and finally, we give a summary and conclusions in Section 4.

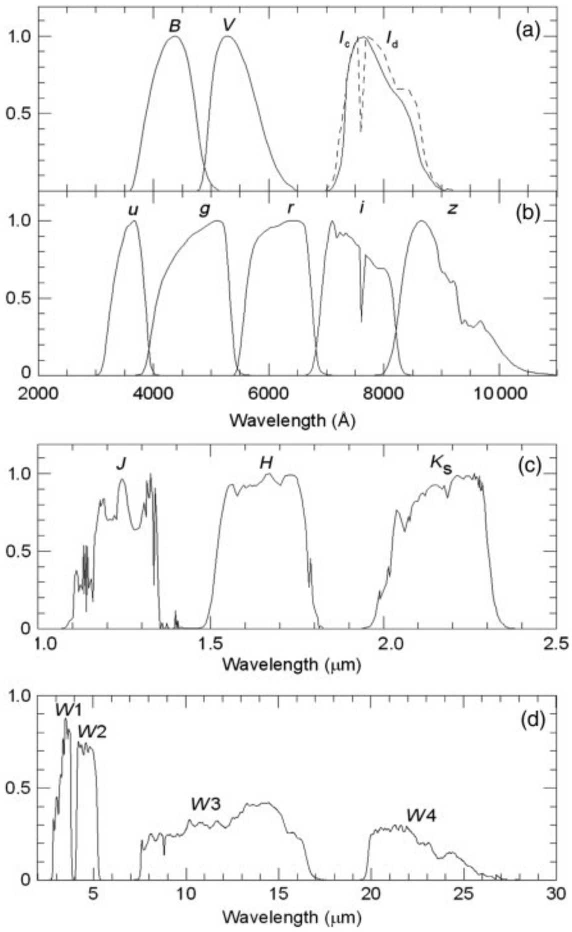

Figure 1 Normalised passbands of the Johnson–Cousins-DENIS filters (a), the SDSS filters (b), the 2MASS filters (c), and the *WISE* filters (d).

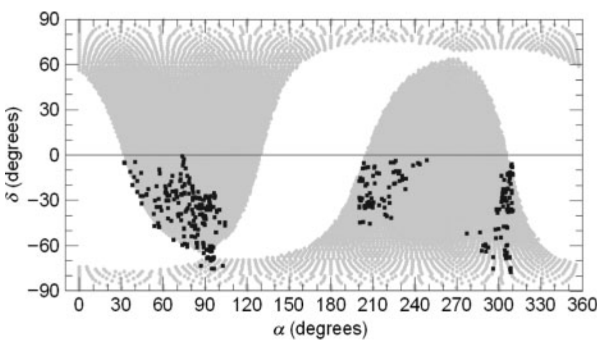

Figure 2 Equatorial coordinates of the stars observed in *WISE* (grey regions) and RAVE (black squares) surveys.

https://doi.org/10.1071/AS11078 Published online by Cambridge University Press

2 The Data

2.1 *RAVE Sample with* Tycho-2*, DENIS, and 2MASS Data*

The main source of our data is the RAVE Data Release (DR3) catalogue (Siebert et al. 2011). The advantage of the RAVE catalogue is that it includes the atmospheric parameters ($T_{\rm eff}$, $\log g$, $[M/H]$) with high accuracy. This is important, as the surface gravity is used to separate the dwarfs and the RC stars and the transformations are derived for different metallicity bins. We initially applied two constraints: $2 < \log g$ (cm s^{-2}) ≤ 3 and $J - H > 0.4$, and obtained a sample of 8003 stars from the RAVE DR3. The reason of these constraints is due to the fact that most of the RC stars lie in this log g interval and that they are much larger in number in the $J - H > 0.4$ colour interval (Bilir et al. 2011b). We then included the following additional but necessary constraints.

1. We selected stars for which *Tycho-2* ($B_{\rm T}$, $V_{\rm T}$), DENIS ($I_{\rm d}$), and 2MASS ($JHK_{\rm s}$) magnitudes were available (3103 stars).
2. We matched the reduced RAVE DR3 catalogue with the *WISE* Preliminary Data Release (PDR) Catalogue[1] and chose the stars which were available with $W1$, $W2$, $W3$, and $W4$ magnitudes (954 stars).
3. We used magnitudes, labeled with 'AAA' flags, which means $S/N \geq 10$, i.e. they have the highest quality measurements, for the 2MASS and *WISE* magnitudes (918 stars).
4. We limited $B_{\rm T} - V_{\rm T}$ colours with $0.8 < (B_{\rm T} - V_{\rm T}) \leq 1.7$ and excluded the stars with $B_{\rm T} - V_{\rm T}$ error larger than 0.2. Thus the complete sample reduced to 355 stars. The $(J - H)_0 - (B - V)_0$ two colour diagram and the spectral distribution of the final sample in three metallicity categories are given in Figure 3.

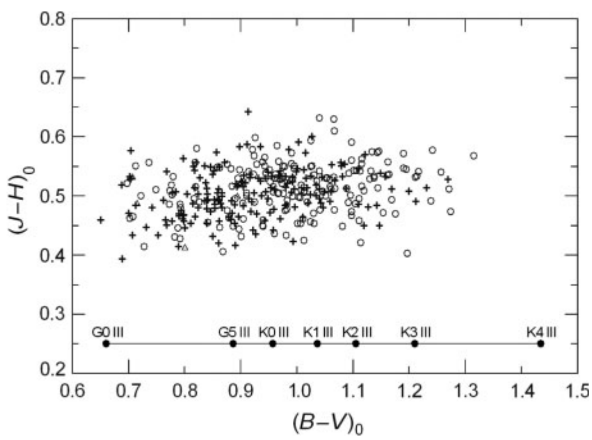

Figure 3 Two colour diagram of the sample stars. The symbols give: (○) $[M/H] > -0.4$, (+) $-1 < [M/H] \leq -0.4$, and (△) $[M/H] \leq -1$ dex.

[1]http://irsa.ipac.caltech.edu/cgi-bin/Gator/nph-scan?mission=irsa&submit=Select&projshort=WISE_PRELIM

2.2 *Evaluating the* BVI$_c$ *Magnitudes*

The RAVE survey does not involve any star observed in the Johnson–Cousins (*BVI*) system. Hence, we have to use the following procedure to obtain B, V, and I magnitudes for our sample: We revealed that 370 stars in the Landolt's (2009) *UBVRI* Photometric Standard Stars catalogue were observed in the DENIS survey (Fouque et al. 2000). We excluded stars with errors in $I_{\rm d}$ larger than 0.1 mag, thus the sample reduced to 355. We matched this sample with the 2MASS catalogue and used magnitudes, labeled with 'AAA' flags, for obtaining the magnitudes of highest quality. This constraint reduced the number of stars to 344.

Finally, we plotted the V magnitudes of Johnson versus the J magnitudes of 2MASS in a two magnitude diagram and eliminated the dwarfs from the sample in Figure 4 (see Bilir et al. 2006, for a description of the elimination method). By doing this, the final giant sample consists of 128 stars.

Figure 4b compares the optical magnitudes of DENIS ($I_{\rm d}$) and Cousins (I) supplied from Landolt (2009). After rejecting four stars which showed large scattering, we obtained the following equation which is used for evaluation of the I (hereafter I) magnitudes of the sample:

$$I = 1.040(\pm 0.007) I_{\rm d} - 0.501(\pm 0.085). \qquad (1)$$

The V magnitudes and $B - V$ colours were evaluated by the following equations taken from the *Hipparcos and Tycho* catalogue (ESA 1997):

$$V = V_{\rm T} + 0.0036 - 0.1284(B_{\rm T} - V_{\rm T}) + 0.0442(B_{\rm T} - V_{\rm T})^2 - 0.015(B_{\rm T} - V_{\rm T})^3, \qquad (2)$$

where

$$(B - V) = \begin{cases} (B_{\rm T} - V_{\rm T}) - 0.113 - 0.258z + 0.40z^3, \\ \quad \text{if} \quad 0.65 < (B_{\rm T} - V_{\rm T}) < 1.1 \\ (B_{\rm T} - V_{\rm T}) - 0.173 - 0.220z - 0.01z^3, \\ \quad \text{if} \quad 1.1 < (B_{\rm T} - V_{\rm T}) \end{cases} \qquad (3)$$

and

$$z = \begin{cases} (B_{\rm T} - V_{\rm T}) - 0.95, & \text{if} \quad 0.65 < (B_{\rm T} - V_{\rm T}) < 1.1 \\ (B_{\rm T} - V_{\rm T}) - 1.20, & \text{if} \quad 1.1 < (B_{\rm T} - V_{\rm T}) \end{cases}. \qquad (4)$$

2.3 *Reddening and Metallicity*

The $E(B - V)$ colour excess of the stars has been evaluated in two steps. First, we used the maps taken from Schlegel, Finkbeiner & Davis (1998) and evaluated a $E_\infty(B - V)$ colour excess for each star. We then reduced

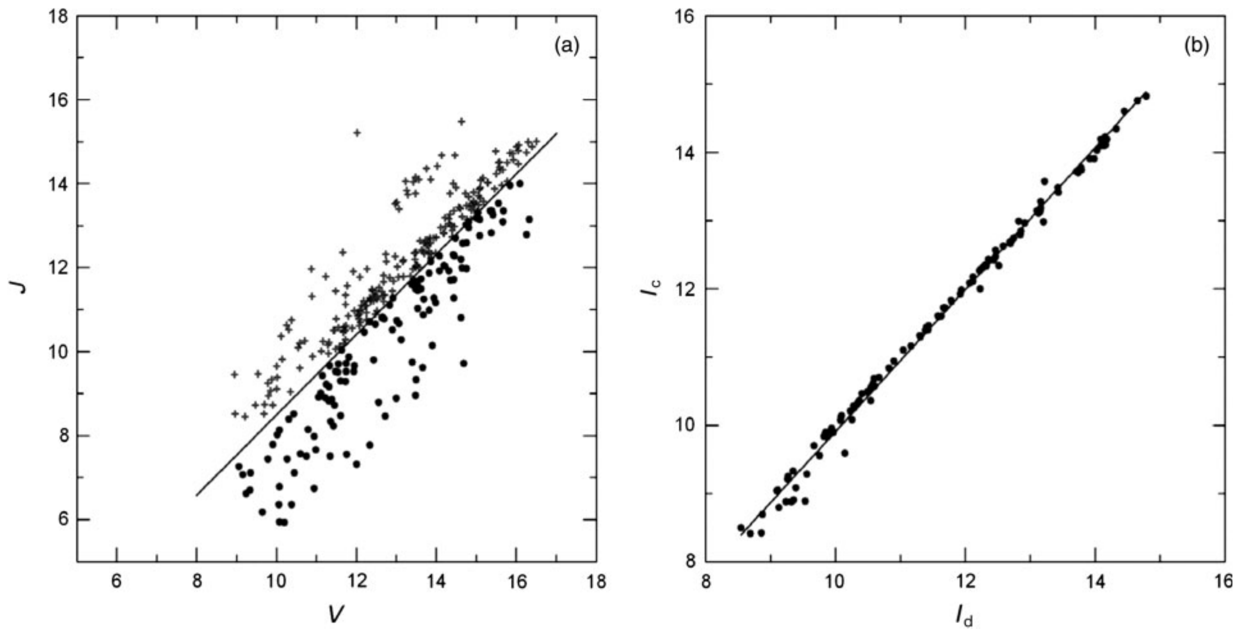

Figure 4 The J versus V two-magnitude diagram for 344 stars observed by Landolt (2009) and the 2MASS survey (panel a) and the two magnitude diagram of Johnson's and DENIS optical magnitudes, I and I_d, for the 124 giants (panel b) identified in panel (a).

them using the following procedure (Bahcall & Soneira 1980):

$$A_d(b) = A_\infty(b)\left[1 - \exp\left(\frac{-|d \times \sin b|}{H}\right)\right]. \quad (5)$$

Here, b and d are the Galactic latitude and distance of the star, respectively. H is the scaleheight for the interstellar dust, which is adopted as 125 pc (Marshall et al. 2006) and $A_\infty(b)$ and $A_d(b)$ are the total absorptions for the model and for the distance to the star, respectively. $A_\infty(b)$ can be evaluated by means of the following equation:

$$A_\infty(b) = 3.1E_\infty(B - V). \quad (6)$$

$E_\infty(B - V)$ is the colour excess for the model taken from the Schlegel et al. (1998). Then, $E_d(B - V)$, i.e. the colour excess for the corresponding star at the distance d, can be evaluated by Equation 7 adopted for distance d,

$$E_d(B - V) = \frac{A_d(b)}{3.1}. \quad (7)$$

As explained in Section 2.1, our sample consists of RC stars. Hence, we adopted the absolute magnitude $M_{K_s} = -1.54 \pm 0.04$ cited by (Groenewegen 2008) and substituted it into the following equation to obtain the distances of the sample stars:

$$(K_s - M_{K_s})_0 = 5\log d - 5 \quad (8)$$

This value has also a small dependence on metallicity and age, hence it can be used accurately in determining the distances to the sources (see Cabrera-Lavers et al. (2007) and references therein for a complete description about using the red clump sources as distance estimators). As the total absorptions for the model and distance to a star are different, $A_d(b)$, and colour excess, $E_d(B - V)$, could be evaluated by iterating Equations 6 to 8.

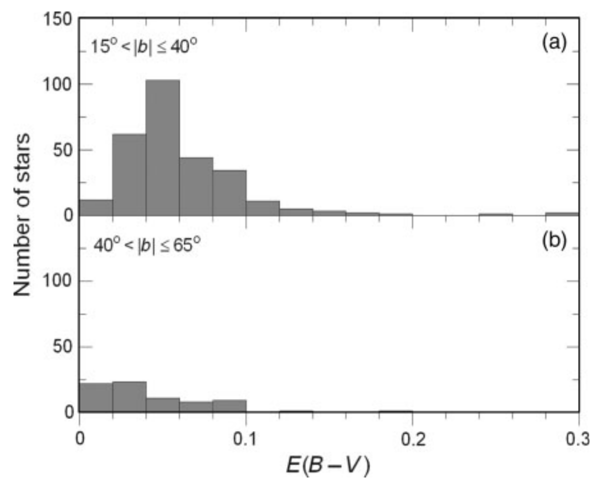

Figure 5 Distribution of colour excess $E(B - V)$.

We have omitted the indices ∞ and d from the colour excess $E(B - V)$ in the equations. However, we use the terms model for the colour excess of Schlegel et al. (1998) and 'reduced' the colour excess corresponding to distance d. The total absorption A_d used in the section and classical total absorption A_V have the same meaning.

We de-reddened the colours and magnitudes by using the $E_d(B - V)$ colour excesses of the stars evaluated using the procedures explained above and the equations of Fan

https://doi.org/10.1071/AS11078 Published online by Cambridge University Press

Table 1. Johnson–Cousins, SDSS, 2MASS and *WISE* magnitudes and colours of the sample stars[a]

Star name	l (deg)[b]	b (deg)[b]	V_0	$(B-V)_0$	$(V-I)_0$	g_0	$(g-r)_0$	$(r-i)_0$	J_0	$(J-H)_0$	$(H-K_s)_0$	$W1_0$	$(W1-W2)_0$	$(W2-W3)_0$	$E_d(B-V)$
T7934_31569_1	2.10152	−28.69877	10.236	1.068	0.917	10.920	0.784	0.260	8.635	0.513	0.118	7.933	−0.097	0.116	0.085
T5031_00326_1	2.46213	+34.06951	15.566	0.804	0.890	11.296	0.749	0.247	9.095	0.503	0.113	8.478	−0.087	0.135	0.169
T7949_00356_1	3.90360	−34.07636	10.651	0.991	1.143	11.082	0.850	0.288	8.646	0.555	0.133	8.024	0.015	0.147	0.047
⋮	⋮	⋮	⋮	⋮	⋮	⋮	⋮	⋮	⋮	⋮	⋮	⋮	⋮	⋮	⋮
⋮	⋮	⋮	⋮	⋮	⋮	⋮	⋮	⋮	⋮	⋮	⋮	⋮	⋮	⋮	⋮
T8396_01656_1	351.88421	−33.13869	10.517	0.921	1.165	11.143	0.874	0.299	8.647	0.579	0.130	7.910	−0.118	0.201	0.041
T8409_01526_1	352.34396	−34.52388	10.510	1.012	1.287	10.864	0.746	0.247	8.651	0.544	0.075	7.939	−0.100	0.158	0.038
T5008_00508_1	354.27874	+45.28820	9.669	0.703	1.053	9.993	0.656	0.209	7.974	0.532	0.023	7.343	−0.031	−0.042	0.183

[a]The complete table is available in electronic format (see Supporting Information).
[b]Galactic coordinates.

Table 2. Mean errors and standard deviations

Filter	Mean error (mag)	s	Photometry
B	0.1155	0.0370	Johnson–Cousins
V	0.0604	0.0161	
I	0.0349	0.0531	
J	0.0246	0.0044	2MASS
H	0.0382	0.0123	
K_s	0.0244	0.0046	
$W1$	0.0246	0.0043	*WISE*
$W2$	0.0216	0.0032	
$W3$	0.0393	0.0098	

(1999) and Fiorucci & Munari (2003) for $V-I$ colour and for the 2MASS photometry:

$$\begin{aligned} V_0 &= V - 3.1E_d(B-V), \\ (B-V)_0 &= (B-V) - E_d(B-V), \\ (V-I)_0 &= (V-I) - 1.250E_d(B-V), \\ J_0 &= J - 0.887E_d(B-V), \\ (J-H)_0 &= (J-H) - 0.322E_d(B-V), \\ (H-K_s)_0 &= (H-K_s) - 0.183E_d(B-V). \end{aligned} \tag{9}$$

As the intrinsic *gri* magnitudes were transformed from the equations of Yaz et al. (2010), no de-reddening was necessary. For de-reddening the magnitudes $W1$, $W2$ and $W3$, we adopted the corresponding total absorptions cited by Bilir et al. (2011a) i.e. $A_{W1}/A_V = 0.051$, $A_{W2}/A_V = 0.030$, and $A_{W3}/A_V = 0.028$, evaluated by means of a spline function fitted to the data of Cox (2000) which cover a range of $0.002 \leq \lambda \leq 250\,\mu$m. Figure 5 shows that the colour excess, $E(B-V)$, is less than 0.1 for most of the stars, and that their distribution peaks at $E(B-V) = 0.05$ mag.

The complete data for the sample of 355 stars are given in Table 1, while the errors for the magnitudes and colours for BVI, JHK_s, and $W1W2W3$ photometric systems are given in Table 2 and Figure 6. As the SDSS magnitudes were transformed from Yaz et al. (2010), we have not shown the corresponding errors in this study. The metallicities are the calibrated values of RAVE DR3. Figure 7 shows that our sample consists mostly of thin and thick disc stars, that present mean metallicities of -0.4 dex (Rocha-Pinto et al. 2006), and -0.7 dex (Cabrera-Lavers, Garzón & Hammersley 2005), respectively. There are only very few stars with $[M/H] < -1$ and $[M/H] > 0.2$ dex, and the mode is at $[M/H] = -0.35$ dex.

3 Results

3.1 Metallicity-Dependent Transformations

We adopted the procedure in Yaz et al. (2010) and used the following general equations to derive nine sets of transformations from *WISE* to Johnson–Cousins, SDSS and 2MASS photometries. As explained in Yaz et al. (2010), this approach, that includes a metallicity term instead of deriving transformations for a set of stars with a metallicity range but omitting the metallicity term, can be

https://doi.org/10.1071/AS11078 Published online by Cambridge University Press

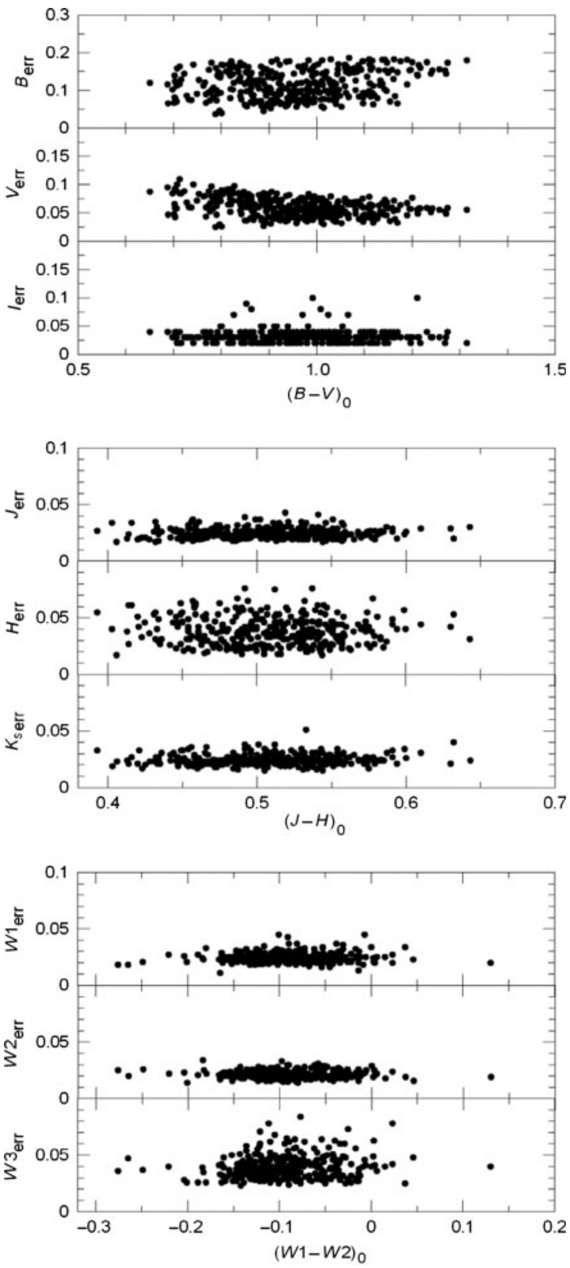

Figure 6 The error distributions for the Johnson–Cousins (*BVI*), 2MASS (JHK_s) and *WISE* (*W*1, *W*2, *W*3) magnitudes.

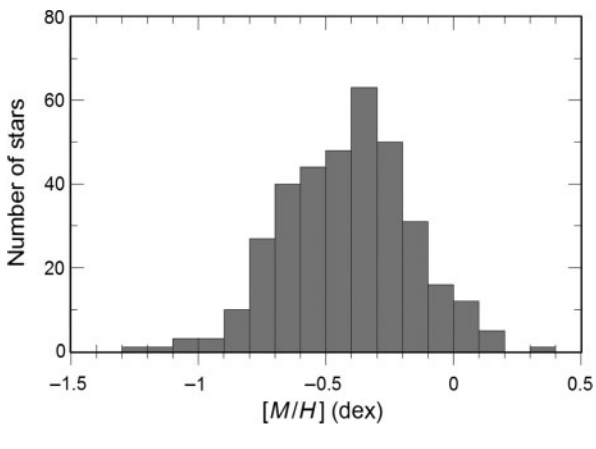

Figure 7 Metallicity distribution for the sample stars.

explained by the fact that stars change their positions in two colour diagrams by shifting an amount proportional to their metallicities. The general equations are as follows:

$$\begin{aligned}
(V-W1)_0 &= a_1(B-V)_0 + b_1(V-I)_0 \\
&\quad + c_1[M/H] + d_1, \\
(V-W2)_0 &= a_2(B-V)_0 + b_2(V-I)_0 \\
&\quad + c_2[M/H] + d_2, \\
(V-W3)_0 &= a_3(B-V)_0 + b_3(V-I)_0 \\
&\quad + c_3[M/H] + d_3, \\
(g-W1)_0 &= a_4(g-r)_0 + b_4(r-i)_0 \\
&\quad + c_4[M/H] + d_4, \\
(g-W2)_0 &= a_5(g-r)_0 + b_5(r-i)_0 \\
&\quad + c_5[M/H] + d_5, \\
(g-W3)_0 &= a_6(g-r)_0 + b_6(r-i)_0 \\
&\quad + c_6[M/H] + d_6, \\
(J-W1)_0 &= a_7(J-H)_0 + b_7(H-K_s)_0 \\
&\quad + c_7[M/H] + d_7, \\
(J-W2)_0 &= a_8(J-H)_0 + b_8(H-K_s)_0 \\
&\quad + c_8[M/H] + d_8, \\
(J-W3)_0 &= a_9(J-H)_0 + b_9(H-K_s)_0 \\
&\quad + c_9[M/H] + d_9.
\end{aligned} \tag{10}$$

The first three sets correspond to the Johnson–Cousins photometry, while the second three and third three sets were derived for SDSS and 2MASS photometries. The numerical values of the coefficients in Equations 10 are given in Table 3.

3.2 Metal-Free Transformations

We also derived metal-free transformations from *WISE* to Johnson–Cousins, SDSS and 2MASS photometries. These can be used to transform the *BVI*, *gri*, and JHK_s data of RC stars with unknown metallicities. Thus we give the chance to the researchers to transfer their *BVI*, *gri*, and JHK_s data with lack of metallicities for RC stars to the *W*1*W*2*W*3 ones. The general equations are as follows:

$$\begin{aligned}
(V-W1)_0 &= \alpha_1(B-V)_0 + \beta_1(V-I)_0 + \gamma_1, \\
(V-W2)_0 &= \alpha_2(B-V)_0 + \beta_2(V-I)_0 + \gamma_2, \\
(V-W3)_0 &= \alpha_3(B-V)_0 + \beta_3(V-I)_0 + \gamma_3, \\
(g-W1)_0 &= \alpha_4(g-r)_0 + \beta_4(r-i)_0 + \gamma_4, \\
(g-W2)_0 &= \alpha_5(g-r)_0 + \beta_5(r-i)_0 + \gamma_5, \\
(g-W3)_0 &= \alpha_6(g-r)_0 + \beta_6(r-i)_0 + \gamma_6, \\
(J-W1)_0 &= \alpha_7(J-H)_0 + \beta_7(H-K_s)_0 + \gamma_7, \\
(J-W2)_0 &= \alpha_8(J-H)_0 + \beta_8(H-K_s)_0 + \gamma_8, \\
(J-W3)_0 &= \alpha_9(J-H)_0 + \beta_9(H-K_s)_0 + \gamma_9.
\end{aligned} \tag{11}$$

The numerical values of the coefficients in Equations 11 are given in Table 3. The comparison between the correlation coefficients *R* and the standard deviations *s* for

https://doi.org/10.1071/AS11078 Published online by Cambridge University Press

Table 3. Coefficients for the transformations

	$i=1$ $(V-W1)_0$	$i=2$ $(V-W2)_0$	$i=3$ $(V-W3)_0$	$i=4$ $(g-W1)_0$	$i=5$ $(g-W2)_0$	$i=6$ $(g-W3)_0$	$i=7$ $(J-W1)_0$	$i=8$ $(J-W2)_0$	$i=9$ $(J-W3)_0$
Metal-dependent transformations									
a_i	0.231 ± 0.056	0.206 ± 0.054	0.228 ± 0.056	12.781 ± 1.272	11.618 ± 0.973	11.513 ± 1.453	1.081 ± 0.056	0.946 ± 0.041	1.004 ± 0.066
b_i	0.859 ± 0.049	0.822 ± 0.047	0.859 ± 0.049	-23.488 ± 3.074	-20.908 ± 2.351	-20.510 ± 3.510	0.695 ± 0.076	0.618 ± 0.056	0.731 ± 0.089
c_i	0.177 ± 0.031	0.161 ± 0.030	0.179 ± 0.031	-0.067 ± 0.013	-0.077 ± 0.010	-0.054 ± 0.015	0.016 ± 0.010	-0.003 ± 0.007	0.019 ± 0.012
d_i	1.367 ± 0.086	1.330 ± 0.083	1.410 ± 0.086	-0.911 ± 0.197	-0.774 ± 0.151	-0.654 ± 0.225	0.057 ± 0.034	0.035 ± 0.025	0.133 ± 0.039
R	0.758	0.754	0.759	0.974	0.983	0.965	0.749	0.795	0.678
s	0.127	0.121	0.127	0.045	0.035	0.052	0.043	0.031	0.050
$<\Delta_{res}>$[a]	−0.00052	0.00014	−0.00017	0.00002	0.00062	0.00084	−0.00009	−0.00016	−0.00022
Metal-free transformations									
α_i	0.362 ± 0.053	0.326 ± 0.051	0.362 ± 0.053	9.301 ± 1.126	7.620 ± 0.900	8.685 ± 1.263	1.102 ± 0.055	0.942 ± 0.040	1.029 ± 0.064
β_i	0.941 ± 0.049	0.897 ± 0.047	0.943 ± 0.049	-15.287 ± 2.745	-11.485 ± 2.193	-13.843 ± 3.078	0.737 ± 0.072	0.610 ± 0.053	0.780 ± 0.084
γ_i	1.082 ± 0.073	1.071 ± 0.070	1.121 ± 0.073	-0.306 ± 0.166	-0.079 ± 0.133	-0.162 ± 0.186	0.035 ± 0.031	0.039 ± 0.022	0.106 ± 0.036
R	0.731	0.729	0.731	0.972	0.980	0.963	0.746	0.794	0.675
s	0.132	0.126	0.132	0.047	0.038	0.053	0.043	0.031	0.050
$<\Delta_{res}>$[a]	0.00128	0.00030	−0.00011	−0.00010	0.00024	−0.00042	−0.00031	0.00010	0.00048

[a]Mean of residual.

Table 4. Coefficients for the inverse transformations

	$i=1$ $(B-W1)_0$	$i=2$ $(V-W1)_0$	$i=3$ $(I-W1)_0$	$i=4$ $(g-W1)_0$	$i=5$ $(r-W1)_0$	$i=6$ $(i-W1)_0$
Metal-dependent inverse transformations						
a_i	2.980 ± 0.212	2.380 ± 0.167	1.480 ± 1.140	3.352 ± 0.124	2.350 ± 0.080	1.945 ± 0.063
b_i	-0.911 ± 0.194	-0.845 ± 0.153	-0.633 ± 0.128	-0.804 ± 0.113	-0.764 ± 0.073	-0.747 ± 0.058
c_i	0.452 ± 0.037	0.264 ± 0.029	0.146 ± 0.024	0.223 ± 0.022	0.136 ± 0.014	0.102 ± 0.011
d_i	1.940 ± 0.111	1.220 ± 0.088	0.620 ± 0.073	1.224 ± 0.065	0.941 ± 0.042	0.882 ± 0.033
R	0.758	0.732	0.624	0.870	0.888	0.899
s	0.168	0.132	0.110	0.098	0.064	0.050
$<\Delta_{res}>$[a]	−0.00070	−0.00109	−0.00121	0.00057	−0.00012	−0.00019
Metal-free inverse transformations						
α_i	3.353 ± 0.251	2.597 ± 0.184	1.598 ± 0.145	3.536 ± 0.140	2.462 ± 0.090	2.129 ± 0.070
β_i	-1.199 ± 0.230	-1.014 ± 0.168	-0.726 ± 0.133	-0.947 ± 0.128	-0.851 ± 0.082	-0.812 ± 0.064
γ_i	1.534 ± 0.127	0.983 ± 0.093	0.489 ± 0.073	1.025 ± 0.071	0.819 ± 0.045	0.791 ± 0.035
R	0.627	0.653	0.570	0.825	0.854	0.872
s	0.200	0.147	0.116	0.112	0.072	0.056
$<\Delta_{res}>$[a]	0.00000	−0.00048	0.00016	−0.00046	0.00005	−0.00055

[a]Mean of residual.

https://doi.org/10.1071/AS11078 Published online by Cambridge University Press

Equations 10 and 11 show that the metallicity dependent transformations are the preferred ones.

3.3 Metallicity-Dependent Inverse Transformations

As was explained before, $W4$ magnitudes cannot be used for the RC star sample. Hence, we adapted the procedure used for dwarfs (Bilir et al. 2011a) to get the metallicity dependent inverse transformations with two colours: By combining linearly the near and mid-infrared colours, $(J-H)_0$ and $(W1-W2)_0$, we transformed them to the optical colours: $(B-V)_0$ and $(V-I)_0$, $(g-r)_0$ and $(r-i)_0$. The general equations are as follows:

$$
\begin{aligned}
(B-W1)_0 &= a_1(J-H)_0 + b_1(W1-W2)_0 \\
&\quad + c_1[M/H] + d_1, \\
(V-W1)_0 &= a_2(J-H)_0 + b_2(W1-W2)_0 \\
&\quad + c_2[M/H] + d_2, \\
(I-W1)_0 &= a_3(J-H)_0 + b_3(W1-W2)_0 \\
&\quad + c_3[M/H] + d_3, \\
(g-W1)_0 &= a_4(J-H)_0 + b_4(W1-W2)_0 \\
&\quad + c_4[M/H] + d_4, \\
(r-W1)_0 &= a_5(J-H)_0 + b_5(W1-W2)_0 \\
&\quad + c_5[M/H] + d_5, \\
(i-W1)_0 &= a_6(J-H)_0 + b_6(W1-W2)_0 \\
&\quad + c_6[M/H] + d_6.
\end{aligned}
\tag{12}
$$

The numerical values of the coefficients in Equations 12 are given in Table 4.

3.4 Metal-Free Inverse Transformations

We adapted the procedure explained in Section 3.3 and derived metal-free inverse transformations between *WISE* and Johnson–Cousins, SDSS photometries. The general equations are as follows, and the numerical values of the coefficients in these equations are given in Table 4:

$$
\begin{aligned}
(B-W1)_0 &= \alpha_1(J-H)_0 + \beta_1(W1-W2)_0 + \gamma_1, \\
(V-W1)_0 &= \alpha_2(J-H)_0 + \beta_2(W1-W2)_0 + \gamma_2, \\
(I-W1)_0 &= \alpha_3(J-H)_0 + \beta_3(W1-W2)_0 + \gamma_3, \\
(g-W1)_0 &= \alpha_4(J-H)_0 + \beta_4(W1-W2)_0 + \gamma_4, \\
(r-W1)_0 &= \alpha_5(J-H)_0 + \beta_5(W1-W2)_0 + \gamma_5, \\
(i-W1)_0 &= \alpha_6(J-H)_0 + \beta_6(W1-W2)_0 + \gamma_6.
\end{aligned}
\tag{13}
$$

Comparison of the correlation coefficients and the standard deviations for Equations 12 and 13 show that the inverse transformations are recommended especially when they are used with a metallicity term as in the direct transformations.

3.5 Residuals

We compared the observed colours with those evaluated by means of the transformations. The residuals corresponding to the Equations 10 and 11 are plotted versus observed colours $(B-V)_0$, $(g-r)_0$, and $(J-H)_0$ in the same figure (Figure 8) with different symbols. For the observed optical colours, the residuals corresponding to the equations just cited are different and they favour the ones with the metallicity term. Whereas for the observed near-infrared colour, i.e. $(J-H)_0$, the two sets of residuals overlap, diminishing the effect of the metallicity term. The same result can be deduced from comparison of the metallicity term c_i $(i=1,\ldots,9)$ in Table 3, where c_i decreases from 0.179 ± 0.031 for $(V-W3)_0$ to -0.003 ± 0.007 for $(J-W2)_0$. The residuals corresponding to the Equations 12 and 13 are plotted versus observed $(W1-W2)_0$ in the same figure with different symbols (Figure 9). The difference between the residuals of two sets are much larger for the ones corresponding to the *BVI* magnitudes relative to the residuals for *gri*. The numerical values of the metallicity term, c_i $(i=1,\ldots,6)$, in Table 4 confirm this suggestion. Actually, $c_1=0.452\pm0.037$ for $(B-W1)_0$ whereas it is only $c_6=0.102\pm0.011$ for $(i-W1)_0$. Hence, we conclude that the metallicity term provides more accurate inverse transformations for *BVI* magnitudes, but that its contribution to *gri* is rather limited.

4 Summary and Conclusions

We have obtained colour transformations for the conversion of *WISE* ($W1W2W3$) magnitudes to the Johnson–Cousins (*BVI*), SDSS (*gri*), and 2MASS (JHK_s) photometric systems, for RC stars. The sample was selected by applying two constraints to the RAVE DR3 data (resulting a sample of 8003 giants): 1) $2<\log g<3\,\mathrm{cm\,s^{-2}}$ and 2) $J-H>0.4$. Matching the coordinates of this sample with the *Tycho-2*, DENIS, 2MASS, and *WISE* catalogues we produced a reduced sample with available magnitudes that is the one used in the transformations. In order to obtain the most accurate transformations, we included four additional constraints: 3) the data were de-reddened, 4) only the stars with high quality were selected, 5) a metallicity term was added to the transformation equations and 6) transformation equations are two-colour dependent; that reduced the total sample to 355 stars.

The transformation equations, and the inverse ones, were designed in two sheets: one with a metallicity term and the other metallicity-free. Comparison between the correlation coefficients and the standard deviations for the two sets promotes the use of the metallicity dependent transformation equations. It is noticeable that even when the procedure used for the transformations for dwarfs was different in Bilir et al. (2008, 2011a), we separated the dwarf sample into different metallicity sub-samples instead of adding a metallicity term to the transformation equations, we obtained here the same result, that is they were metallicity dependent. This dependence of the transformations on metallicity had been also confirmed in Yaz et al. (2010).

As in the case of dwarfs, *WISE* has an advantage relative to the 2MASS photometric system due to its deeper magnitudes. Actually, $W1$ is a magnitude deeper than K_s for sources with spectra close to an A0 star and

https://doi.org/10.1071/AS11078 Published online by Cambridge University Press

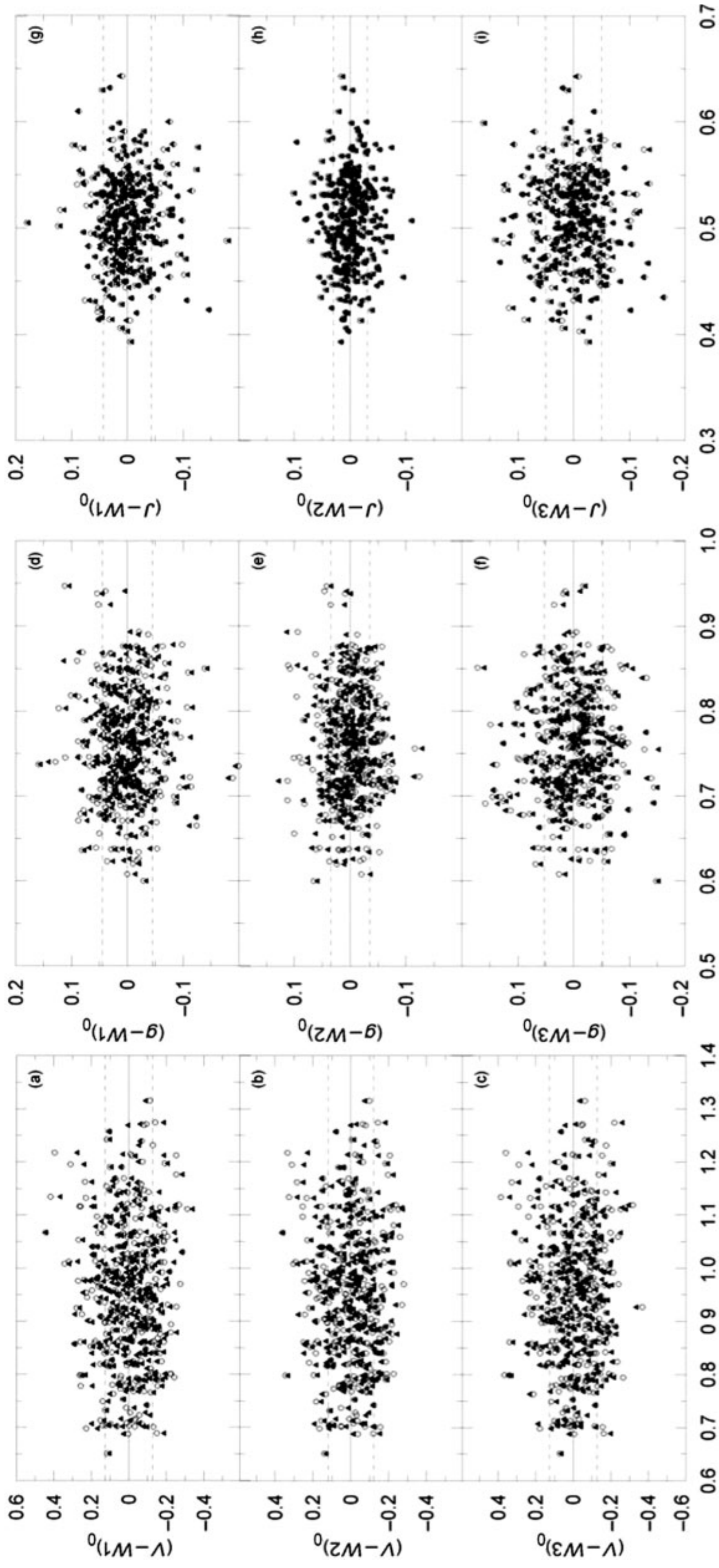

Figure 8 Colour residuals for the metallicity-dependent (○) and metal free (▲) transformations. The notation used is △(colour) = (evaluated colour) − (observed colour). The horizontal dashed lines correspond to 1σ residuals. (a) – (c) for BVI_c, (d) – (f) for SDSS, and (g) – (i) for 2MASS photometric system.

https://doi.org/10.1071/AS11078 Published online by Cambridge University Press

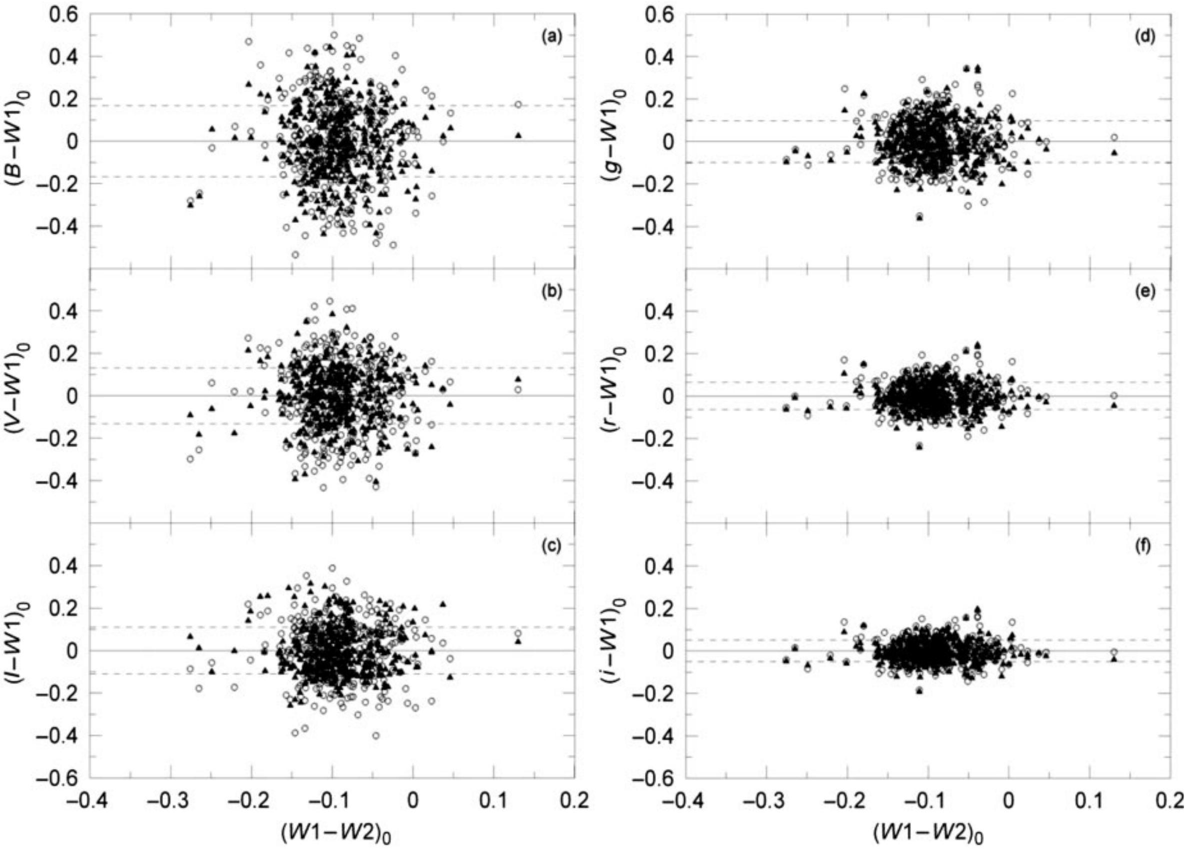

Figure 9 Colour residuals for the metallicity dependent (○) and metal free (▲) inverse transformations. The notation used is △(colour) = (evaluated colour) – (observed colour). The horizontal dashed lines correspond to 1σ residuals. (a) – (c) for BVI_c, and (d) – (f) for SDSS photometric system.

even deeper for *K* and *M* spectral stars. The present transformations can be applied to stars with known absolute *V*, *g*, or *J* magnitudes, when absolute magnitudes for *W*1 can be also provided. These two advantages can be used to investigate the RC stars in the thin and thick discs more accurately, and combining this study with the one carried out for dwarfs would be even more fruitful. A possible interesting application of the transformations presented here would be the comparison of the (new) Galactic model parameters and the ones estimated in situ, but the transformations also can be used in a wide variety of research fields.

Acknowledgments

This work has been supported in part by the Scientific and Technological Research Council (TÜBİTAK) 111T650.

Funding for RAVE has been provided by: the Australian Astronomical Observatory; the Leibniz-Institut fuer Astrophysik Potsdam (AIP); the Australian National University; the Australian Research Council; the French National Research Agency; the German Research Foundation; the European Research Council (ERC-StG 240271 Galactica); the Istituto Nazionale di Astrofisica at Padova; The Johns Hopkins University; the National Science Foundation of the USA (AST-0908326); the W. M. Keck foundation; the Macquarie University; the Netherlands Research School for Astronomy; the Natural Sciences and Engineering Research Council of Canada; the Slovenian Research Agency; the Swiss National Science Foundation; the Science & Technology Facilities Council of the UK; Opticon; Strasbourg Observatory; and the Universities of Groningen, Heidelberg and Sydney. The RAVE web site is at `http://www.rave-survey.org`.

This research has made use of the NASA/IPAC Infrared Science Archive and Extragalactic Database (NED) which are operated by the Jet Propulsion Laboratory, California Institute of Technology, under contract with the National Aeronautics and Space Administration.

This publication makes use of data products from the Two Micron All Sky Survey, which is a joint project of the University of Massachusetts and the Infrared Processing and Analysis Center/California Institute of Technology, funded by the National Aeronautics and Space Administration and the National Science Foundation.

This research has made use of the SIMBAD, and NASA's Astrophysics Data System Bibliographic Services.

References

Aihara, H., et al., 2011, ApJS, 193, 29
Bahcall, J. N. & Soneira, R. M., 1980, ApJS, 44, 73
Bilir, S., Karaali, S., Güver, T., Karataş, Y. & Ak, S., 2006, AN, 327, 72

https://doi.org/10.1071/AS11078 Published online by Cambridge University Press

Bilir, S., Ak, S., Karaali, S., Cabrera-Lavers, A., Chonis, T. S. & Gaskell, C. M., 2008, MNRAS, 384, 1178
Bilir, S., Karaali, S., Ak, S., Dağtekin, N. D., Önal, Ö., Yaz, E., Coşkunoğlu, B. & Cabrera-Lavers, A., 2011a, MNRAS, 417, 2230
Bilir, S., Karaali, S., Ak, S., Önal, Ö., Coşkunoğlu, B. & Seabroke, G. M., 2011b, MNRAS, 418, 444
Cabrera-Lavers, A., Garzón, F. & Hammersley, P. L., 2005, A&A, 433, 173
Cabrera-Lavers, A., Hammersley, P. L., González-Fernández, C., López-Corredoira, M., Garzón, F. & Mahoney, T. J., 2007, A&A, 465, 825
Cox, A. N., 2000, Allen's Astrophysical Quantities (New York: AIP Press)
ESA, 1997, The Hipparcos and Tycho Catalogues ESA SP-1200 (Noordwijk: ESA), 61
Fan, X., 1999, AJ, 117, 2528
Fiorucci, M. & Munari, U., 2003, A&A, 401, 781
Fouque, P., et al., 2000, A&AS, 141, 313
Groenewegen, M. A. T., 2008, A&A, 488, 25
Keenan, P. C. & Barnbaum, C., 1999, ApJ, 518, 859
Landolt, A. U., 2009, AJ, 137, 4186
Marshall, D. J., Robin, A. C., Reylé, C., Schultheis, M. & Picaud, S., 2006, A&A, 453, 635
Padmanabhan, N., et al., 2008, ApJ, 674, 1217
Puzeras, E., Tautvaišienė, G., Cohen, J. G., Gray, D. F., Adelman, S. J., Ilyin, I. & Chorniy, Y., 2010, MNRAS, 408, 1225
Rocha-Pinto, H. J., Rangel, R. H. O., Porto de Mello, G. F., Bragança, G. A. & Maciel, W. J., 2006, A&A, 453, L9
Schlegel, D. J., Finkbeiner, D. P. & Davis, M., 1998, ApJ, 500, 525
Siebert, A., et al., 2011, AJ, 141, 187
Skrutskie, M. F., et al., 2006, AJ, 131, 1163
Steinmetz, M., et al., 2006, AJ, 132, 1645
Wright, E. L., et al., 2010, AJ, 140, 1868
Yaz, E., Bilir, S., Karaali, S., Ak, S., Coşkunoğlu, B. & Cabrera-Lavers, A., 2010, AN, 331, 807
York, D. G., et al., 2000, AJ, 120, 1579
Zwitter, T., et al., 2008, AJ, 136, 421